Tribol Lett (2008) 30:1–11
DOI 10.1007/s11249-008-9304-7

ORIGINAL PAPER

Initiation of Sliding of an Elastic Contact at a Nanometer Scale Under a Scanning Force Microscope Probe

Pierre-Emmanuel Mazeran · Moez Beyaoui

Received: 9 October 2006 / Accepted: 1 February 2008 / Published online: 16 February 2008

Abstract A contact between a scanning force microscope Si_3N_4 probe and a flat surface of similar material is created. The low roughness of surfaces and their mechanical properties allow generating a nanoscopic elastic contact governs by an extended Hertz theory (DMT theory). The behavior of the initiation of sliding is investigated by submitting the contact to lateral sinusoidal displacements whose amplitude increases from zero to a few nanometers. The lateral force generated by the displacement is analyzed by a lock-in amplifier and the in-phase and out-of-phase components are recorded as a function of the displacement amplitude. Experimental results are compared to the Mindlin and Savkoor theories, which describe the initiation of sliding of macroscopic elastic contact. A relatively good agreement between our experiments and these theories is observed. For our particular experimental conditions, i.e., Si_3N_4 probe sliding on a similar material, the Mindlin's model gives a slightly better agreement than the Savkoor's model. This study shows that macroscopic concepts remain valid at the nanoscale, at least for the particular case studied here.

Keywords Nanotribology · Static friction · AFM · Energy conservation

1 Introduction

Friction and wear are an everyday issue and are implied in many industrial processes and natural phenomena from earthquakes dynamics to physics of granular media. From an industrial point of view, the energy losses by friction must be reduced to decrease the economic and ecological impacts or to increase the autonomy of portable mechanical systems. Nevertheless, the fundamental phenomena governing friction and wear remain insufficiently understood. These phenomena are particularly difficult to investigate due to the fact they include mechanical and physico-chemical aspects of surfaces for which the natures and geometries are not completely controlled. For example, the relations between the friction force, the real contact area, the sliding velocity, and the adhesion force remain too badly explained in front of the scientific stakes [1, 2].

The development of the scanning force microscope (SFM) [3, 4] and surface force apparatus (SFA) [5, 6] offers new opportunities for the understanding of friction, wear, and adhesion at a nanometer scale. The major advantage of these instruments is to be able to generate contacts with a good control of the geometrical (shape and roughness), mechanical, and physico-chemical operating conditions. It is thus possible to obtain single asperity contacts and to reach the governing laws of this kind of contact. Many studies were carried out on single asperity contacts [2–7]. Linear relations between friction force and contact area [8–10] or applied load [8, 10, 11] have been observed, meaning that the shear stress is constant or depends on contact pressure. The influence of sliding velocity on friction force were studied and showed a logarithmic increase or decrease of friction force with increasing velocity [12–16].

In this article, initiation of sliding is particularly investigated. Experimental results show that for a single asperity nanoscopic contact that complies with the Hertz theory and Amontons's law, the initiation of sliding, in our operating conditions, still complies with the theory described by Mindlin [17, 18].

P.-E. Mazeran (✉) · M. Beyaoui
Laboratoire Roberval, Unité de Recherche en Mécanique, UMR CNRS-UTC 6253, Université de Technologie de Compiègne, BP 60319, 60206 Compiegne Cedex, France
e-mail: mazeran@utc.fr

2 Initiation of Sliding in a Hertzian Contact

The Hertz theory was established at the end of the 19th century [19] to describe the characteristics of an elastic contact between two curved surfaces without roughness. In the case of a contact between a sphere of radius R and a plan, the main relations between the characteristics of the contact such as the contact radius a ($a \ll R$), the indentation depth h, the relative displacement of the center of the two bodies in contact δ, the load F, and the maximum contact pressure $P_{\max}$ are given by the following relations:

$$a = \sqrt[3]{\frac{3}{4}\frac{RF}{E^*}} \tag{1}$$

$$\delta = 2h = \frac{a^2}{R} = \sqrt[3]{\frac{9}{16}\frac{F^2}{RE^{*2}}} \tag{2}$$

$$P_{\max} = \frac{3}{2}\frac{F}{\pi a^2} = \frac{1}{\pi}\sqrt[3]{\frac{6F^2E^{*2}}{R^2}} \tag{3}$$

where E^* is the combined Young's modulus

$$\frac{1}{E^*} = \frac{1-\nu_1^2}{E_1} + \frac{1-\nu_2^2}{E_2} \tag{4}$$

E is the Young's modulus and ν the Poisson's ratio of the materials of the two bodies in contact.

When a contact between two spheres is submitted to a relative displacement, there is initially a shear for displacements much lower than the contact radius. The lateral force is then proportional to the displacement d:

$$F_L = k_L d \tag{5}$$

where k_L the lateral contact stiffness equals to:

$$k_L = 8aG^* \tag{6}$$

and G^* is the reduced shear modulus:

$$\frac{1}{G^*} = \frac{2-\nu_1}{G_1} + \frac{2-\nu_2}{G_2} \tag{7}$$

where G_i is the shear modulus of the materials of the two bodies in contact.

Mindlin [17, 18] investigated the problem of the initiation of sliding in an elastic contact between two spheres that complies with the Hertz theory and Amontons's law [20]:

$$\mu = \frac{F_F}{F} \tag{8}$$

where F_F is the friction force and μ the friction coefficient. During the initiation of sliding, he suggests that when the relative displacement d increases, there is an increase of the lateral force F_L and of the shear stress that causes a partial sliding of the contact: An increasing annulus at the periphery of the contact slides whereas the center of the contact of radius c is sheared (Fig. 1).

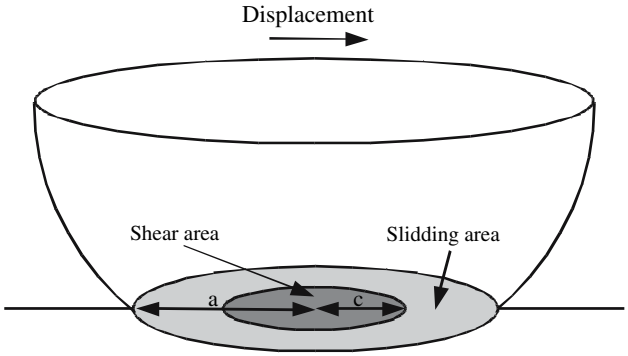

Fig. 1 Initiation of sliding in an elastic contact. According to the Mindlin or Savkoor theory, the initiation of sliding is progressive: While the displacement d increases, an increasing annulus at the periphery of the contact slides whereas the center of the contact of radius c is sheared

$$\frac{c}{a} = \sqrt{1 - \frac{F_L}{F_F}} \tag{9}$$

The lateral force F_L should not be confused with the friction force: It is the sum of the sheared force of the contact's center and of the friction force of the sliding contact's periphery. The lateral force evolves from a shear force to a friction force as the relative displacement increases. During the initiation of sliding, the lateral force is not proportional to the displacement as observed in a stick-slip model ($F_L = k_L d$ if $d < F_F/k_L$, $F_L = F_F$ if $d \geq F_F/k_L$).

As the relative displacement d increases, the sliding area increases and the sheared area decreases. Sliding is total when the relative displacement d reaches a critical value D. The relation between the lateral force and displacement is given by the Mindlin equation:

$$\begin{aligned} &\frac{F_L}{F_F} = 1 - \left(1 - \frac{d}{D}\right)^{3/2}, \quad \text{if } d < D \\ &F_L = F_F, \quad \text{if } d > D \end{aligned} \tag{10}$$

with

$$D = \frac{3}{2}\frac{F_F}{8aG^*} \tag{11}$$

Savkoor [21] proposed a different approach of the initiation of sliding for a friction force proportional to the contact area. The relation between the lateral force and the displacement is equal to:

$$\begin{aligned} &\frac{F_L}{F_F} = \frac{2}{\pi}\left(a\cos\left(\sqrt{1-\left(\frac{d}{D}\right)^2}\right)\right. \\ &\qquad \left. + \frac{d}{D}\sqrt{1-\left(\frac{d}{D}\right)^2}\right), \quad \text{if } d < D \\ &F_L = F_F, \quad \text{if } d > D \end{aligned} \tag{12}$$

with

$$D = \frac{4}{\pi}\frac{F_F}{8aG^*} \quad (13)$$

For an oscillating displacement, these equations are still valid but the boundaries conditions change leading to more complex equations.

3 Experiments and Results

3.1 Method

The initiation of sliding can be easily highlighted by a simple measurement of the lateral force as a function of the displacement. In the case of a SFM, the measurement of the lateral force is done easily using a simple measurement of the torsion of the SFM cantilever [22]. The calibration of the lateral force is relatively easy to make with the help, for example of a sample presenting known slopes [23]. It is the exact control of displacements that is cumbersome. Indeed, in SFM experiments, a piezo scanner makes displacements. The piezo scanner has the advantage of proposing a resolution of displacements much lower than the atomic dimension. Nevertheless, it has the drawback to give a strongly nonlinear response characterized by strong hysteresis and a creep effect. If one seeks to initiate sliding by starting a relative displacement of the ceramic, the relation between the input voltage and the exact displacement will not be known. The curve of the lateral force according to displacement will be erroneous due to a bad knowledge of the real displacement. Any comparison with a theoretical model will be impossible.

We chose to impose a sinusoidal voltage to the piezo scanner in order to have a better control of the displacements by feeding the SFM piezo scanner at only one frequency and to measure the amplitude of the lateral force. This method has already been used successfully to measure friction force and lateral contact stiffness at a nanometer scale [24–29].

A commercial SFM is modified by implementing displacement optical sensors in the three space directions. The experimental device and its applications will be described in another paper [30]. A short description is given here: The principle of this homemade displacement sensor is the following [31, 32]. A fixed optical fiber emits light near a mobile mirror. Light is reflected by the mirror, reaches optical reception fibers surrounding the emission fiber, and is guided to a PIN photodiode (Fig. 2). The amount of light received by these reception fibers is a function of the distance between the fibers and the mobile mirror. The displacement sensor has a sensitivity of about 30 mv/μm and a linear response (non-linearity <1% full-scale output) for a displacement range of 200 μm. The RMS noise of the sensor is about 2 nm. The calibration of the displacement is achieved by calculating the sensitivity of the scanner for some fixed frequencies.

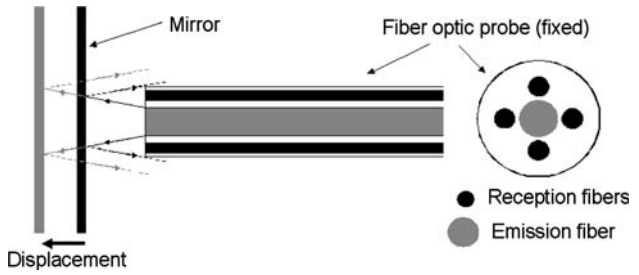

Fig. 2 Schematic principle of the displacement sensor used to calibrate the piezo-scanner displacement

- The sensor is first calibrated for quasi-static displacement by comparing the response of the sensor according to the calibrated displacement of the piezo scanner. A triangular scan of 30 μm at 1 Hz is imposed to the scanner and the sensor voltage is measured. The sensor voltage is proportional to the displacement that allows calculating the sensitivity of the sensor.
- In a second step, the scanner is calibrated for sinusoidal displacements at various frequencies. The use of a lock-in-amplifier allows increasing significantly the signal-to-noise ratio by filtering the sensor signal. Experimental data show that when one imposes a sinusoidal voltage to the piezo scanner, the displacement is sinusoidal. The phase between displacement and voltage is constant at a fixed frequency and is independent of the voltage amplitude. The displacement (by means of the voltage sensor) as a function of the scanner voltage is quasi-linear (non-linearity <1%) from a few nanometers to a few micrometers. The sensitivity of the scanner can then be determined at a fixed frequency by calculating the slope of the curve displacement/scanner voltage.

The calibration of the scanner sensitivity for harmonic displacements is done indirectly with a calibration grating and a lock-in-amplifier. The inaccuracy of the calibration is mainly due to calibration grating and lock-in-amplifier uncertainties. We estimate the uncertainty of the calibration to be less than 5%.

The cross-coupling phenomenon has been checked. When one imposes a sinusoidal displacement in the Y direction (parallel to the surface and perpendicular to the main axis of the cantilever), a relative sinusoidal displacement is observed in the other directions. Typically, cross-coupling for frequency in the 1 Hz–2 kHz range is about 0.7 ± 0.3% and 1.1 ± 0.3% in the X and Z directions, respectively, and could be neglected.

To investigate the initiation of sliding, we propose to make a relative sinusoidal displacement of the contact ($d = d^*\sin(\omega t)$) whose half-amplitude d^* varies from zero to several nanometers. A sinusoidal voltage is imposed to the scanner in the Y direction and converted into a sinusoidal displacement using the sensitivity of the scanner at the considered frequency. The signal of the lateral force generated by the displacement of the contact is sent to a lock-in amplifier. The lock-in amplifier acts like a filter and takes into account only the first harmonic of the lateral force signal at the frequency of the imposed displacement. It provides the half-amplitude, Amp, and the phase, ϕ, of the first harmonic components of the lateral force signal. They can be transformed into an in-phase component F'_L and an out-of-phase component F''_L of the first harmonic of the lateral force.

$$F'_L = \text{Amp}\cos(\phi) \tag{14}$$

$$F''_L = \text{Amp}\sin(\phi) \tag{15}$$

The experimental response can be compared to the theoretical response. The theoretical response of the contact can be computed from the Eqs. 10 and 12 in the case of the Mindlin, Savkoor, or a stick-slip model that can be observed in SFM experiments especially for atomic flat surfaces [33]. Figure 3 shows the relative lateral force (F_L/F_F) as a function of an oscillating relative displacement of various half-amplitude according to the Mindlin theory ($d^*/D = 1/3$, 1, and 2). For $d^*/D = 1/3$, the lateral force is approximately proportional to the displacement: The contact is mainly sheared as sliding is limited to the contact periphery. For higher displacement, the lateral force is proportional to the displacement only at the beginning of the displacement and is equal to the friction force for displacement value superior to D. The theoretical signal of the lateral force generated by a sinusoidal displacement is computed for d^*/D values varying from zero to infinity. The first harmonic F_1 of the relative lateral force ($F_1 = \text{Amp}\sin(\omega t + \phi)$) is computed as a function of d^*/D. Figure 4 shows the relative lateral force signal as a function of time for various d^*/D values. For $d^*/D = 1/3$, the contact is mainly sheared and the lateral force is approximately proportional to the displacement. The lateral force is then sinusoidal and in phase with the displacement. For $d^*/D = 2$, the contact slides and the lateral force signal is truncated at the value of the friction force and becomes a square signal. The half-amplitude of the first harmonic of the lateral force signal is then superior to the value of the friction force and its phase is in advance from the displacement (Fig. 4). When the displacement tends to infinity, the half-amplitude of the first harmonic of the lateral force tends to $4/\pi$ the value of the friction force and the phase tends to $\pi/2$ [25]. By varying d^*/D, it is possible to

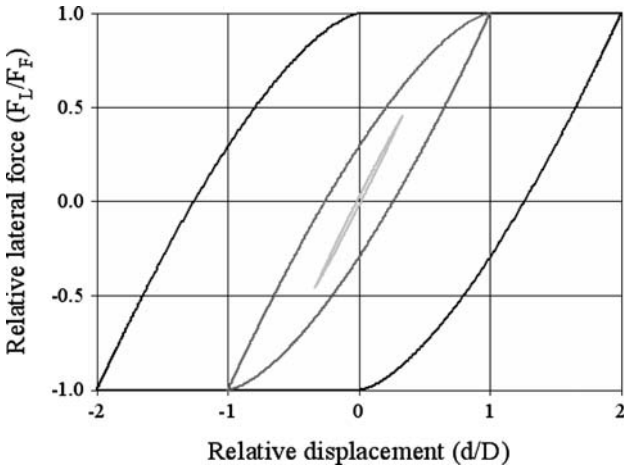

Fig. 3 Normalized lateral force as a function of an oscillating normalized displacement according to the Mindlin theory. For low displacement half-amplitude ($d^*/D = 1/3$, light gray curve), the contact is sheared and the lateral force is approximately proportional to the displacement. For higher displacement half-amplitude ($d^*/D = 1$, gray curve; $d^*/D = 2$ black curve), the contact begins to slide and the lateral force is no more proportional to the displacement

compute the half-amplitude, Amp, and phase, ϕ, as well as the in-phase (Amp $\cos(\phi)$) and out-of-phase (Amp $\sin(\phi)$) components of the first harmonic of the relative lateral force. To get the correct values of the lateral force, the amplitude should be divided by a correction factor χ. The values of χ vary from 1 to $4/\pi$ as a function of the normalized half-amplitude displacement d^*/D ($\chi = f(d^*/D)$) but are only slightly sensitive to the considered theory: the maximum difference between the correcting factors for the two theories (Mindlin or Savkoor) for a fixed value of d^*/D is lower than 0.3%. Figure 5 shows the theoretical phase and normalized lateral force (lateral force divided by the friction force) as a function of d^*/D. Figure 6 shows the theoretical normalized in-phase and out-of-phase components of the lateral force as a function of d^*/D.

This method of measurement of the initiation of sliding and more generally of friction has some advantages:

1. The response of the contact could be computed on a great number of cycles. Then, an average response is obtained leading to more significant value.
2. The response of the contact is done on contact area of a few tens of nanometer square than one can regard as homogeneous.
3. The method allows working with high sliding velocity. Indeed, by carrying out displacements of the order of the micrometer at high frequencies (a few kHz), it is possible to obtain sliding velocities of several mm/s. These velocities are difficult to obtain in classical SFM experiments for which the velocity is of the order of the μm/s. Thus, the method allows us to increase the

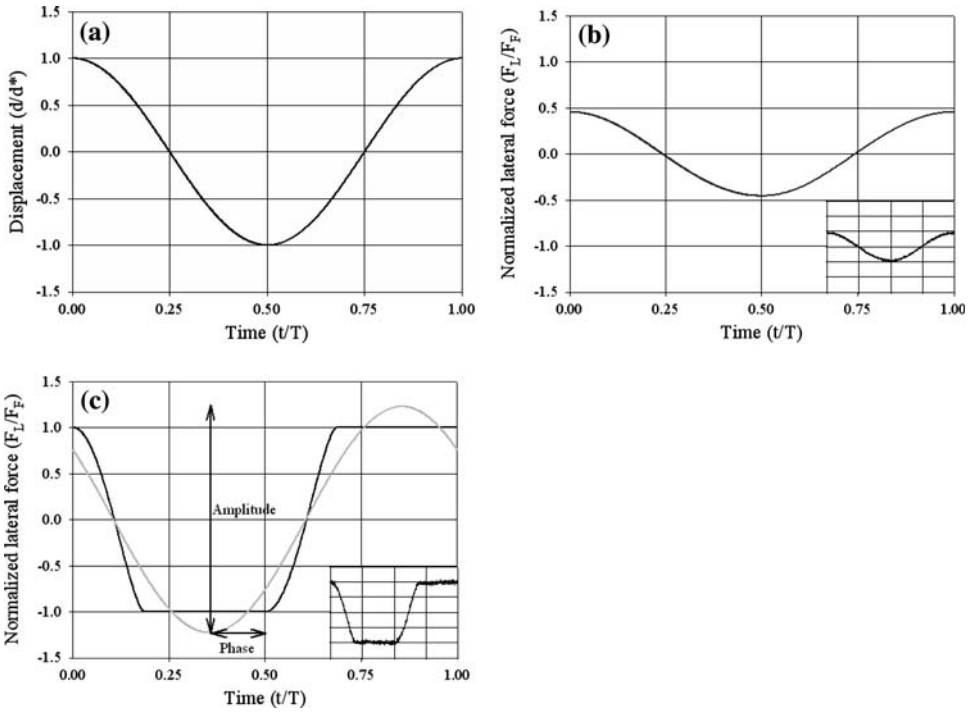

Fig. 4 Lateral force and its first harmonic as a function of time (t/T where T is the period of the harmonic displacement) for a contact submitted to a sinusoidal displacement of various half-amplitude (d^*/D). (**a**) Displacement (d/d^*) as a function of time. (**b**) For a low displacement half-amplitude ($d^*/D = 1/3$), the lateral force is a sinusoidal pattern in phase with the displacement. The inset is an experimental curve ($d^*/D \approx 1/3$). (**c**) For a higher displacement half-amplitude ($d^*/D = 2.5$) the first harmonic (gray line) of the lateral force (black line) has a half-amplitude superior to the friction force and is in advance of phase. The inset is an experimental curve ($d^*/D \approx 2.5$)

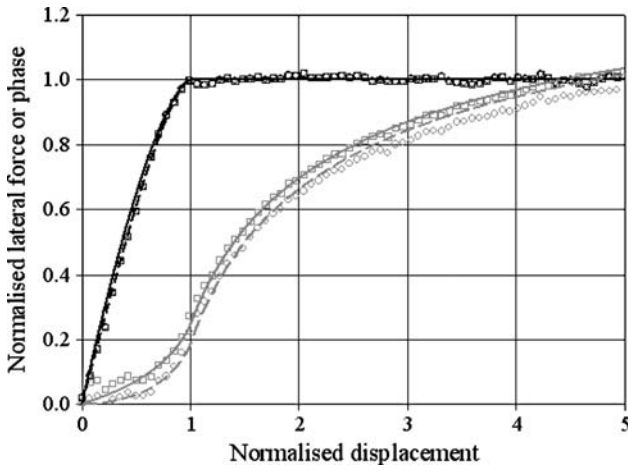

Fig. 5 Normalized lateral force (F_L/F_F) and phase as a function of the normalized displacement amplitude (d^*/D). Black lines are the lateral forces, gray lines are the phases, solid lines are Mindlin curves, dashed lines are Savkoor curves, squares are experimental data fitted with Mindlin model, and circles are experimental data fitted with Savkoor model. Note that the two experimental curves of the normalized lateral force are confused

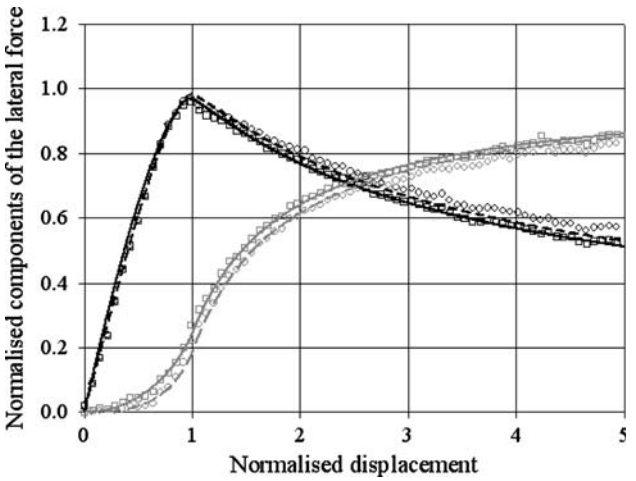

Fig. 6 Normalized in-phase and out-of-phase component of the lateral force (F_L/F_F) as a function of the normalized displacement amplitude (d^*/D). Black lines are in-phase component, gray lines are out-of-phase component, solid lines are Mindlin curves, dashed lines are Savkoor curves, squares are experimental data fitted with Mindlin model, and circles are experimental data fitted with Savkoor model

sliding velocity by several orders of magnitude and to obtain measurements of friction on several decades.

4. The dynamic experiments allow to have two information, the amplitude and the phase (or the in-phase and out-of-phase component) of the lateral force. The sum of the in-phase component of all the harmonics of the signal of the lateral force is proportional to the stored energy W_S (i.e., mainly the shear energy of the contact), divided by the displacement amplitude. In the same way, the sum of the out-of-phase component of all the harmonics of the signal of the lateral force is proportional to the dissipated energy W_D (mainly by friction), divided by the displacement amplitude. Then, this method allows reaching to the ratio of the stored to the dissipated energy. This is obviously of major interest for the study of the initiation of sliding that is a transition from shear (stored elastic energy) to friction (dissipated energy): As a first approximation, by

estimating that the elastic energy of the contact is similar to the elastic energy of a spring, we can calculate the stored energy:

$$W_S \approx \frac{1}{2} k_L a^2 = 4G^* a^3 \quad (16)$$

and the dissipated energy by friction in the sliding domain ($d^* > D$) equals to

$$W_D \approx (d^* - D) F_F \quad (17)$$

If we consider that the first harmonic of the lateral force is a good estimate of the lateral force, the phase of the lateral force in the sliding domain is approximately equal to:

$$\phi \approx \tan^{-1}\left(\frac{W_D}{W_S}\right) \approx \tan^{-1}\left(\frac{(d^* - D)F_F}{4G^* a^3}\right) \quad (18)$$

In the case of a Mindlin contact, by introducing Eqs. 1 and 8, Eq. 18 becomes:

$$\phi \approx \tan^{-1}\left(\frac{(d^* - D)\mu E^*}{3RG^*}\right) \quad (19)$$

The phase is only sensitive to d^* if the other parameters are constant. In our method, increasing d^* is equivalent to increase the sliding velocity. If μ is not constant as a function of the displacement, as proposed by several models [34, 35], the phase could be used as an indicator of the variation of the friction during the initiation of sliding. The fact to have two data, the amplitude and the phase of the lateral force, is a very good indicator of the relationship between the friction force and the contact area. This method is then very useful to study the relationship between contact area, friction force, and sliding velocity.

Nevertheless, this method presents some drawbacks. The first one is related to the fact that the initiation of sliding is done after several cycles that can cause during the experiment changes of the operating conditions (plastic flow, wear, heat, change of the physico-chemical conditions…). The other one is related to the fact that the sliding velocity is not constant during the experiment. This can introduce artifacts of measurements particularly if the friction force is dependent of the sliding velocity. It is, for example, known that the friction force at a nanometric scale shows a great dependence on the sliding velocity [2].

3.2 Contact Between Two Silicon Nitride Surfaces

To establish a contact that comply with both Hertz theory and Amontons's law, Si_3N_4 cantilevers were used (DNP, Digital Instruments, USA). The probe has a nominal curvature radius equal to 20 nm. The most rigid cantilever was used to avoid artifacts. The nominal stiffness of the cantilevers is 0.58 N/m.

In order to make a contact of the simplest nature, we chose to establish a contact between the probe and a flat surface of similar nature in order to have the same materials for the two bodies in contact. The back of a chip of a DNP cantilever was chosen. An environmental scanning electron microscope (ESEM) analysis shows that the chemical natures are similar for the cantilever and the center of the chip. One will note nevertheless the presence of oxygen and carbon in the Si_3N_4 layer. The silicon nitride is manufactured by CVD technique, starting from a mixture of ammonia and dichloro-silane. Its chemical composition is variable and the ratio N/Si varies from 0.27 to 1.33 [36]. The mechanical properties of the silicon nitride were measured with the help of nanoindentation testing. The tests were performed with a Nanoindenter XP (MTS, USA) using a Berkovitch indenter and the Oliver & Pharr method [37] at constant strain rate (0.05 s^{-1}) until a maximum indentation depth of 1,000 nm. Experiments have been conducted using the 'Continuous Stiffness Measurement' method that allows a continuous measurement of the Young's modulus and Hardness. The Young's modulus and the hardness were found to be constant from 150 to 400 nm indentation depths. Young's modulus and hardness were measured to be 140 and 25 GPa, respectively. This result is in accordance with reported results for which the value of the Young's modulus varies from 130 to 155 GPa [23, 36].

After experiments, the probe radius was measured to be 26 ± 5 nm using an ESEM microscope. Due to the non-conductive nature of Si_3N_4, probe imaging is difficult and the measurement leads to a high uncertainty on the probe radius. In situ calibration of the probe radius [38, 39] failed to give reliable result as images realized in contact mode are too noisy. The total displacement during an experiment of the initiation of sliding is approximately 600 μm. This distance is equivalent of the displacement done for a 1 μm^2 image. Furthermore, silicon nitride is known to be resistant to wear. Then during a set of experiments the wear of the probe radius could be neglected and the probe radius could be considered to be constant.

The cantilever stiffness was estimated using the unloaded resonant frequency [40]. The resonant frequency was found to be equal to 59.21 kHz. According to the geometrical and material properties of the cantilever, its stiffness could be estimated to be equal to 0.65 N/m. Cantilever calibration is a difficult task especially for silicon nitride cantilever. Burnham et al. [41] compared the results of four different calibration methods and found important discrepancies. The cantilever stiffness is then estimated with a high inaccuracy leading to a poor accuracy of the applied load.

The friction force calibration has been done using the in situ method proposed by Ogletree et al. [23]. A copper surface chemically polished is used as sample for calibration. The method allows calibrating the friction coefficient,

meaning that the friction force/normal force ratio is known with a good uncertainty (<5%).

3.3 Initiation of Sliding

The aim of this article is to show that the initiation of sliding at the nanometer scale still complies with macroscopic theory without expanding on the validity of the Hertz theory and the Amontons's law in our experimental conditions. This last aspect has nevertheless been studied and the validity of the Hertz theory and Amontons's law was checked (see Appendix for details).

The experiments of the initiation of sliding have been done with a commercial SFM (Dimension 3100, Digital Instruments, USA). For the experiments presented in this article, the normal force was equal to 90 nN. The adhesive force was measured to be 28 nN leading to a total applied force equal to about 118 nN. The displacements were generated at a frequency of 500 Hz from zero to a few nanometers and the amplitude and phase of the lateral force were recorded.

Experimental data are fitted to the theoretical curves by adjusting the value of the friction force (59 nN), of D (0.18 nm), and of the phase of the lateral force signal.

In a first step, a constant value ϕ_0 is added to the experimental phase ϕ in order to get the corrected phase ϕ'. We assume that when the d^* is close to zero, there is no dissipation in the contact (no sliding) and then the phase ϕ' should be equal to zero. Then, the value of ϕ_0 is chosen in order to have an experimental phase very close to the theoretical one especially when d^* tends to zero $\left(\underset{d^*\to 0}{\phi'} = \phi - \phi_0 = 0\right)$: The introduction of ϕ_0 is necessary to correct the phase between the displacement of the piezo-scanner and the input voltage.

In a second step, the out-of-phase component of the lateral force is plotted as a function of the in-phase component of the lateral force and fitted to the theoretical curve by adjusting the value of the friction force. Then, in a third step, the in-phase and out-of-phase components of the lateral force are plotted as a function of d^* and fitted to the theoretical curves by adjusting the value of D. In a last step, the experimental data are corrected using the correcting factor χ in order to obtain the true value of the lateral force.

Figure 5 shows the half-amplitude and phase of the lateral force as a function of the d^*/D, and Fig. 6 shows the in-phase and out-of-phase components of the lateral force as a function of d^*/D. A very good agreement between experimental and theoretical data according to the Mindlin theory is observed. The experimental data are also compared with the Savkoor theory using a different value of ϕ_0. Whatever the value of ϕ_0, it is not possible to fit the amplitude, phase, in-phase, and out-of phase components with the same agreement. This is particularly obvious for large displacements; in this case the experimental data of the phase, in-phase, and out-of-phase component are clearly lower than the theoretical values. If a higher value of ϕ_0 is chosen, the agreement is good for large value but fails for low value of d^*/D. The phase is an indicator of the ratio of the dissipated energy to the stored energy. The fact that the theoretical phase is lower for a Savkoor model means that the shear energy is higher for this model. As total sliding occurs, the shear energy increase becomes constant while the dissipated energy increases linearly with displacement. The phase as a function of the displacement curves are then different for the two theories and are not a simple shift. The fact that the fit for Savkoor curve is less good seems to show that this model does not plan the correct shear energy.

The Mindlin and the Savkoor models are very similar; the lateral force as a function of the normalized displacement is very close for the two models and could not be detected for a quasi-static displacement. But for an oscillating displacement, the use of the amplitude and the phase allows comparing the quality of the agreement between experimental results and the two theories. Obviously the difference between the two theories is so weak that it is difficult to conclude definitively that the Savkoor model is not valid in our experimental conditions as the experimental curve could be sensitive to artifacts (nonlinearity of the signals, noncurve geometry of the probe, etc...). Nevertheless, the fact that the fit seems better for the Mindlin model and that the friction force is proportional to load (see Appendix for details) made us confident in the fact that the Mindlin theory is still valid for our experimental conditions. Whatever, this experiment shows that the initiation of sliding in a nanometer contact could be also described by theories developed for macroscopic contact.

The fitting value of D for the Mindlin theory is equal to 0.18 nm. According to the value of the friction force (59 nN) and the calculated value of G^* (16 GPa), the contact radius is computed to be 3.8 nm (3.2 nm for a Savkoor model). One should notice that the values used to fit experimental data are given with an uncertainty due to the difficulty to calibrate signals at high frequencies. Furthermore, the fitting value of D is not perfectly constant from an experiment to another. Nevertheless, the experimental contact radius is in good agreement with the theoretical value (3.1 nm) calculated using Eq. 1. The uncertainty of the values of probe radius, applied load (and then cantilever stiffness), and reduced Young's modulus are high, leading to a high uncertainty (at least 50%) of the theoretical value of the contact radius. The uncertainty of D and then the experimental contact radius is only due to the uncertainty of the displacement, the friction force, and the

combined shear modulus. These errors are systematic and lead to a constant error on the contact radius. The present method is then interesting to measure experimentally the contact radius with a constant uncertainty. This data is generally impossible to obtain and we propose to use it for the determination of the contact area.

The fitting value of the friction force is also in relative good agreement with the experimental friction force. The experimental friction force is obtained by means of the half-amplitude of the lateral force divided by $\pi/4$. This value is obtained during an oscillating displacement of high amplitude (about 4 nm at 500 Hz) for the same applied load. The values are 59 and 65 nN for the fitting and experimental values, respectively.

4 Discussion

Mindlin supposed that the friction force complies with Amontons's law, meaning that friction force is proportional to both area and stress:

$$F_{\mathrm{F}} = \int \tau P \, \mathrm{d}A \tag{20}$$

He decomposed the contact area in two components: The shear area is the center of the contact and the sliding area, the periphery. The energy needed to move the contact is only stored by shear or dissipated by friction. If one considers only the first harmonic of the signal and neglect the others harmonics, the in-phase and out-of-phase components of the lateral force are proportional to the stored and dissipated energy, respectively. The excellent agreement between experiments and theory shows that the experimental dissipated and stored energy is similar to those predicted by the Mindlin theory. In conclusion, the ratio of the shear area to the sliding area follows those predicted by the Mindlin theory and friction force complies with Amontons's law as experimentally observed (see Appendix for details).

These experimental results are quite easy to obtain, reproducible, and are not affected by changes in the applied load or frequency. It is especially true at low frequencies for which the data are integrated on a few numbers of cycles. No change of behavior was observed for low applied forces for which the contact could be a multi asperities contact. The principal reason is that it was not possible to achieve experiments under negative load due to snap-off (contact are maintained only by adhesive force). Further experiments will be conducted in a liquid environment to resolve this technical problem.

The Mindlin and Savkoor theories are not universal as they do not consider adhesion forces. Johnson has proposed theoretical model about the influence of the adhesion force on the friction force [34, 35]. He shows that the contact radius is not constant from static to sliding friction leading to a different mechanism of the initiation of sliding than the Mindlin or Savkoor theory. Initiation of sliding experiments conducted on a polycarbonate surface shows a poor agreement with the Mindlin or Savkoor theory [30], suggesting that the Savkoor–Briggs and Johnson models should be considered. Further works on the initiation of sliding on polymer will be done to investigate the validity of these models.

In the present experimental case the adhesion is mainly due to capillary force. Adhesion forces are not able to deform the surface and the contact still complies with an extended Hertz theory (DMT model, see Appendix for details). Experimentally, there is no evidence that the capillary force changes from shear to sliding even for displacement well higher than the contact radius. As the two bodies in contact are rigid, the contact radius (about 3 nm) is about three times lower than the radius of the circular wet area r_1 (about 9 nm).

$$r_1 = \sqrt{2\, r_{\mathrm{K}} R} \tag{21}$$

The agreement between the Mindlin theory and experiments being excellent, we can conclude that the adhesion force is constant during the experiments. This means that the meniscus bridge between the two surfaces slides as the contact slides without significant change of the contact area or that the sliding velocity of the contact is lower than the velocity of (re)formation of the water meniscus. Nevertheless, for higher frequencies (6 kHz) and higher amplitudes (few tens of nanometers) and then higher sliding velocities, discrepancies were observed between the Mindlin theory and experiments. This discrepancy is characterized by a fall of the in-phase and out-of-phase components of the lateral force with an increasing velocity. These falls could be related to a decrease of the total applied load due to a fall of the adhesion force. This aspect has been developed in another article [42].

5 Conclusion

Experimental results show that in our operating conditions and for a nanometer-size contact between two silicon nitride surfaces, the DMT and Amontons's laws are still valid. A dynamic method to investigate the initiation of sliding is used by submitting the contact to an oscillating displacement $d = d_0 \cos(\omega t)$ of increasing amplitude. The in-phase and out-of phase components of the first harmonic of the lateral force signal are measured and compared with the theoretical values of a Mindlin and Savkoor model. A relatively good agreement between our experiments and these theories is observed. For our particular experimental conditions, the Mindlin's model gives a slightly better

agreement than the Savkoor's model. This study shows that macroscopic concepts remain valid at the nanoscale, at least for the particular case studied here.

Appendix: Conditions for using DMT Theory and Amontons's Law in a Nanoscale Contact

We seek to establish a contact that complies with both Hertz theory and Amontons's law theories with a SFM probe. It is thus necessary that some assumptions are checked:

1. The contact must be perfectly elastic without plastic deformation. For that, it is necessary that the hardness of surfaces is large compared to the contact pressure.
2. Surfaces must be sufficiently flat to not modify the Hertzian geometry of the contact. The Hertz theory is based on surfaces without roughness that is difficult to valid at a nanometer scale. It is thus necessary to check that the surface roughness can be neglected. We propose to compare the roughness of the surfaces of the theoretical contact area with the theoretical indentation depth (Fig. 7). If the roughness of the theoretical contact area is weak compared to the theoretical indentation depth, the surface asperities are deformed elastically and that the contact is governed by the Hertz theory. On the other hand, if the roughness is large compared to the theoretical indentation depth, it is difficult to imagine that the surface asperities are deformed elastically to form a single asperity contact: The contact will thus be done between the asperities of the two surfaces. The Hertz law can thus be validated.
3. The presence of a capillary meniscus generates the presence of adhesive force that can form an adhesive neck. This neck increases the contact area and generates a contact that complies with the JKR theory. It is thus necessary to check that the elastic deformation is negligible compared to the range of the capillary forces.

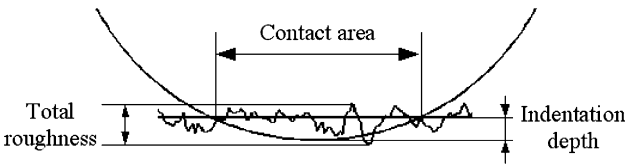

Fig. 7 Comparison between the indentation depth and the contact roughness. The theoretical indentation is calculated for a contact between a sphere and a flat surface and is compared with the total roughness in the same area. If the total roughness is well lower than the indentation depth, it becomes obvious that the asperities are flattened out and that the contact could be considered as a single asperity contact. At the opposite, if the total roughness is high compared to the indentation depth, the asperities are not flattened out and the contact should be considered as a polyasperities contact

4. Lastly, the Mindlin theory is based on a linear relation between the friction force and the normal force (Amontons's law). It is thus necessary to check that the friction force is proportional to the normal force.

Elasticity of the Contact

In order to confirm the elastic nature of the contact, the theoretical contact stress is compared to the hardness of the sample. If one supposes that the contact complies with the Hertz theory, the required force F_{lim} to have a maximal contact stress equal to the hardness H is:

$$F_{\text{lim}} = \frac{\pi^3 H^3 R^2}{6E^{*2}} \tag{22}$$

If we take the measured mechanical properties of the silicon nitride ($H = 25$ GPa, $E^* = 75.5$ GPa taking $\nu = 0.27$ [23]) and the nominal probe radius ($R = 26$ nm), the required force to generate plastic flow is equal to 9,600 nN. This force is well superior to the highest force used during the experiments and the hypothesis that the contact remains fully elastic is valid.

Validity of the Hertzian Theory for Rough Surfaces

We propose to compare the theoretical indentation depth with the roughness of the theoretical contact area. Indeed, roughness parameters are highly dependent on the considered area [43]. For large considered area, the roughness parameters like the Arithmetic Roughness R_{A} and the Mean Square Roughness R_{MS} are generally constant. For low considered area, the roughness parameter follows a power relationship to the considered area. The measurement of the surface roughness in the contact area is particularly difficult due to its very small value. The theoretical contact radius is of the order of a few nanometers. At this scale, it is difficult to measure accurately the topography for two reasons: first, the probe radius is big compared to the considered area leading to an artifact known as dilation [38]; second, for low roughness the noise-to-signal ratio becomes high. These two phenomena do not allow measuring the true topography of the surfaces. Nevertheless, we propose to estimate the roughness of the contact area by extrapolating the roughness measured at larger scales.

A topographic image of the silicon nitride surface was made using a sharp probe (TESP-NCL, Nanosensors, Switzerland) in order to reduce the dilation phenomenon. The so-called Soft Tapping imaging mode was used and servo loop parameters were fixed as low as possible to optimize the noise-to-signal ratio.

The parameter R_{MS} is then computed as a function of the considered area: The image is cut up in square part of

decreasing size. For each part of the image, the R_{MS} is computed. Then, for all parts of the image of similar size, the median values of the R_{MS} are calculated and plotted as a function of the considered area.

As the height of the surface follows a Gaussian distribution, six times the RMS roughness corresponds to 99.7% of the distribution and could be considered as a good approximation of the value of the total roughness R_T (difference between the highest and the lowest point). Then, it is judicious to compare this value to the theoretical indentation depth h of a contact of same area A. The indentation depth is equal for a Hertzian contact to:

$$h = \frac{a^2}{2R} = \frac{A}{2\pi R} \tag{23}$$

Figure 8 shows on the same graph the estimated roughness $R_T = 6\ R_{MS}$ and the theoretical indentation depth h of a contact area A as a function of its contact radius a ($a = (A/\pi)^{1/2}$). The indentation depth is superior to the roughness for a limit value of 2.7 nm. This value corresponds to an applied force equal to about 100 nN. The probability to generate a single asperity contact is superior to 1/2 for a force superior to 100 nN.

Obviously, due to the very small-scale value of the contact area, the estimation of the roughness in this area is poorly accurate and underestimated by the high noise-to-signal ratio. For forces superior to 100 nN, the probability to have a single asperity contact superior to 1/2 is concluded.

Capillary Adhesion in an Elastic Contact

The Hertz theory showed its robustness in many experimental cases [44] including at the nanometer scale [2–7]. However, in some experimental cases, the adhesion force cannot be neglected. In ambient air, the presence of water generates the formation of a capillary meniscus around contacts [45–47], the main adhesion force is due to the attractive force generated by this capillary meniscus.

As a function of the ratio of the elastic strain with the range of the adhesion force, the JKR theory [47] or the DMT theory [48] governs the contact. Maugis [49] has studied the transition between the DMT and JKR theories using a Dugdale model [50] for which the depression due to adhesion σ_0 is constant if the distance between surfaces is lower than a threshold value and null beyond that. Maugis introduces a dimensional parameter λ:

$$\lambda = 2\sigma_0 = \sqrt[3]{\frac{9R}{16\pi w E^{*2}}} \tag{24}$$

and shows that the DMT and JKR theories are valid if $\lambda < 0.1$ and $\lambda > 3$, respectively. The Dudgale model is perfectly adapted to capillary condensation. If one modifies

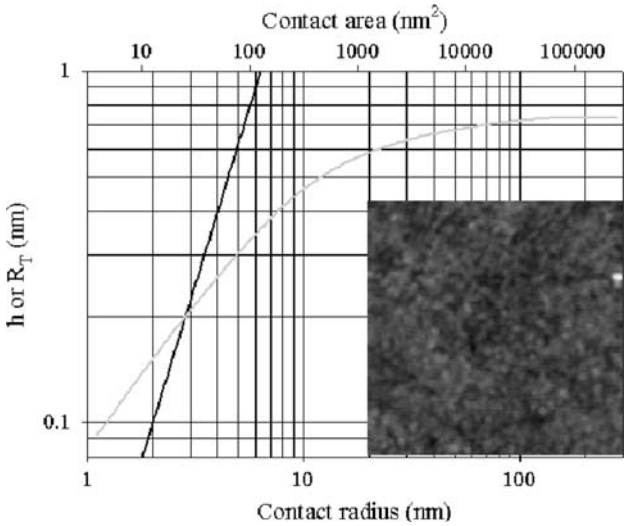

Fig. 8 Comparison between the theoretical indentation depth (black line) and the average total roughness by means of six times the RMS roughness (gray line) in a contact of area A as a function of the contact radius a. The roughness is computed from the inset SFM image. The theoretical indentation depth becomes superior to the total roughness for contact radius equals to approximately 2.7 nm. This contact radius is theoretically achieves for a total applied force close to 100 nN

the parameter of Maugis to the case of capillary condensation ($\sigma_0 = \Delta P = -\gamma_{LV}/r_K$ and $w = 2\gamma_{LV}$), one obtains:

$$\lambda = -\frac{1}{r_K}\sqrt[3]{\frac{9R\gamma_{LV}^2}{4\pi E^{*2}}} \tag{25}$$

In the case of capillary adhesion, the numerical applications show that the Maugis criterion is close to zero for current relative humidity (30–60%) and current SFM probes (R = 10–40 nm). Exception occurs for very low Young's modulus ($E < 1$ GPa) for which the Maugis or JKR theories are more adapted.

During experiments, the humidity was typically between 30 and 60% leading to a Kelvin's radius between −1 and −2.3 nm, the nominal probe radius 20 nm and the combined Young's modulus equal to 75.5 GPa. The calculation of the Maugis parameter λ applied to a capillary force has been done using Eq. 25 and a value between 0.010 and 0.024 has been found. This value shows us without ambiguity that the DMT theory is valid in our experimental conditions.

Validity of the Amontons's Law

The relationship between the friction force and the normal force is measured by means of the present method with displacement half-amplitude well higher than the contact radius ($d^* \gg D$). At these displacement half-amplitudes, the value of the half-amplitude of the first harmonic of the lateral force signal is close to $4/\pi$ the value of the friction

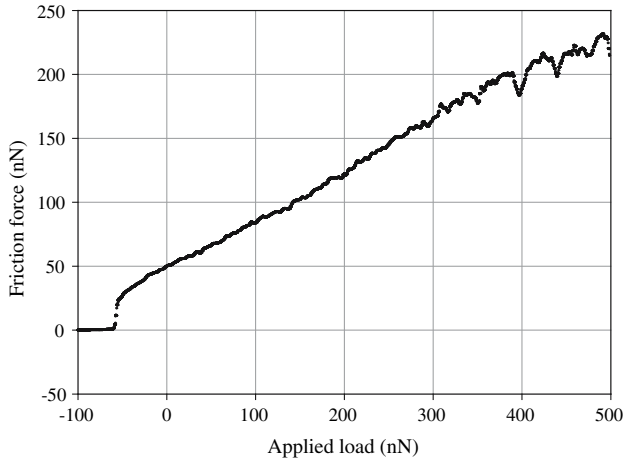

Fig. 9 Dynamic friction force as a function of the applied load. The friction force (by means of the half-amplitude of the lateral force divided by $\pi/4$) is proportional to the normal force but not equal to zero at snap-off. This phenomenon is due to the oscillating displacement that generates a premature snap-off

force [25, 28, 29]. The friction force by means of the half-amplitude of the lateral force divided by $\pi/4$ is proportional to the normal force (Fig. 9). The friction force is not equal to zero at snap-off. This phenomenon is due to the oscillating displacements that generate a premature snap-off: The adhesive force was measured to be well lower when the probe is submitted to a lateral oscillating displacement. The Amontons's law is then valid in our experiments.

References

1. Bushan, B.: Micro/Nanotribology and its Applications. Kluwer Academic Publishers, Dordrecht (1997)
2. Meyer, E., Overney, R.M., Dransfeld, K., Gyalog, T.: Nanoscience: Friction and Rheology on the Nanometer Scale. World Scientific, London, UK (1998)
3. Binnig, G., Quate, C.F., Gerber, C.: Phys. Rev. Lett. **56**, 930 (1986)
4. Mate, C.M., McClelland, G.M., Erlandsson, R., Chiang, S.: Phys. Rev. Lett. **59**, 1942 (1987)
5. Israelachvili, J., Guiggan, P.M.: Science **241**, 795 (1988)
6. Tonck, A., Georges, J.-M., Loubet, J.-L.: J. Colloid Interface Sci. **125**, 150 (1988)
7. Carpick, R.W., Salmeron, M.: Chem. Rev. **97**, 1963 (1997)
8. Schwarz, U.D., Allers, W., Gensterblum, G., Wiesendanger, R.: Phys. Rev. B **52**, 14976 (1995)
9. Carpick, R.W., Agrait, N., Ogletree, D.F., Salmeron, M.: J. Vac. Sci. Technol. B **14**, 1289 (1996)
10. Schumacher, A., Kruse, N., Prins, R., Meyer, E., Lüthi, R., Howald, L., Güntherodt, H.J., Scandella, L.: J. Vac. Sci. Technol. B **14**, 1264 (1996)
11. Piétrement, O., Troyon, M.: Langmuir **17**, 6540 (2001)
12. Riedo, E., Levy, F., Brune, H.: Phys. Rev. Lett. **88**, 185505-4.1 (2002)
13. Bouhacina, T., Aimé, J.P., Gauthier, S., Michel, D., Heroguez, V.: Phys. Rev. B **56**, 7694 (1997)
14. Zwörner, O., Holscher, H., Schwarz, U.D., Wiesendanger, R.: Appl. Phys. A **66**, S263 (1998)
15. Gnecco, E., Bennewitz, R., Gyalog, T., Loppacher, Ch., Bammerlin, M., Güntherodt, H.J.: Phys. Rev. Lett. **84**, 1172 (2000)
16. Liu, H., Ahmed, S.I.U., Scherge, M.: Thin Solid Films **381**, 135 (2001)
17. Mindlin, R.D.: Trans. ASME Serie E J. Appl. Mec. **16**, 259 (1949)
18. Mindlin, R.D., Mason, W.P., Osmer, J.F., Deresiewicz, H.: Proc. 1st US National Congress of Applied Mechanics, New York, USA, 203 (1951)
19. Hertz, H.: J. Reine Angew. Math. **92**, 156 (1882)
20. Amontons, G.: Mémoire de l'Académie Royale A 257 (1706)
21. Savkoor, A.R., Briggs, G.A.D.: Proc. R. Soc. Lond. A **356**, 103 (1977)
22. Meyer, G., Amer, N.M.: Appl. Phys. Lett. **53**, 2400 (1988)
23. Ogletree, D.F., Carpick, R.W., Salmeron, M.: Rev. Sci. Instrum. **67**, 3298 (1996)
24. Goddenheinrich, T., Muller, S., Heiden, C.: Rev. Sci. Instrum. **65**, 2870 (1994)
25. Colchero, J., Luna, M., Baro, A.M.: Appl. Phys. Lett. **68**, 2896 (1996)
26. Carpick, R.W., Ogletree, D.F., Salmeron, M.: Appl. Phys. Lett. **70**, 1548 (1997)
27. Lantz, M.A., O'Shea, S.J., Welland, M.E., Johnson, K.L.: Phys. Rev. B **55**, 10776 (1997)
28. Piétrement, O., Troyon, M.: Tribol. Lett. **7**, 213 (1999)
29. Mazeran, P.-E., Loubet, J.-L.: Tribol. Lett. **7**, 199 (1999)
30. Mazeran, P.-E.: To be submitted to Rev. Sci. Instrum.
31. Kissinger, C.: Fibre optic displacement measuring apparatus. US Patent 3,940,608 (1967)
32. Prelle, C., Lamarque, F., Mazeran, P.-E.: J. Eur. Syst. Autom. **36**, 1295–1307 (2002)
33. Morita, S., Fujisawa, S., Sugawara, Y.: Surf. Sci. Rep. **23**, 1 (1996)
34. Johnson, K.L.: Proc. R. Soc. Lond. A **453**, 163 (1997)
35. Sader, J.E., Larson, I., Mulvaney, P., White, L.R.: Rev. Sci. Instrum. **66**, 3789 (1995)
36. (a) Petersen, K.E., Guarnieri, C.R.: J. Appl. Phys. (b) Petersen, K.E.: Proc. IEEE **70**, 420 (1982)
37. Oliver, W.C., Pharr, G.M.: J. Mater. Res. **7**, 1566 (1992)
38. Villarrubia, J.S.: J. Res. Natl. Inst. Stand. Technol. **102**, 425 (1997)
39. Mazeran, P.E., Odoni, L., Loubet, J.L.: Surf. Sci. **585**, 25 (2005)
40. Cleveland, J.P., Manne, S., Bocek, D., Hansma, P.K.: Rev. Sci. Instrum. **64**, 403 (1993)
41. Burnham, N.A., Chen, X., Hodges, C.S., Matei, G.A., Thoreson, E.J., Roberts, C.J., Davies, M.C., Tendler, S.J.B.: Nanotechnology **14**, 1 (2003)
42. Mazeran, P.-E.: Mater. Sci. Eng. C **26**, 751 (2006)
43. Tricot, C., Ferland, P., Baran, G.: Wear **172**, 127 (1994)
44. Johnson, K.L.: Contact Mechanics. Cambridge University Press, Cambridge, UK (1984)
45. Weisenhorn, A.L., Khorshandi, M., Kasas, S., Gotzos, V., Butt, H.J.: Nanotechnology **4**, 106 (1993)
46. Israelachvili, J.N.: Intermolecular and Surface Forces, 2nd edn. Academic Press, London, UK (1991)
47. Johnson, K.L., Kendall, K., Roberts, A.D.: Proc. R. Soc. Lond. A **324**, 301 (1971)
48. Derjaguin, B.V., Muller, V.M., Toporov, Y.P.: J. Colloid Interface Sci. **53**, 314 (1975)
49. Maugis, D.: J. Colloid Interface Sci. **150**, 243 (1992)
50. Dugdale, D.S.: J. Mech. Phys. Solids **8**, 100 (1960)